Construction and Building Materials 284 (2021) 122786

Contents lists available at ScienceDirect

Construction and Building Materials

journal homepage: www.elsevier.com/locate/conbuildmat

Temperature and humidity influence on the strain sensing performance of hybrid carbon nanotubes and graphite cement composites

Beatriz del Moral [a], F. Javier Baeza [a], Rosa Navarro [a], Oscar Galao [a], Emilio Zornoza [a], Jose Vera [b], Catalina Farcas [a], Pedro Garcés [a,*]

[a] Department of Civil Engineering, University of Alicante, Carretera San Vicente s/n, 03690, San Vicente del Raspeig, Spain
[b] ACCIONA Construction S.A., Technological Center, Valportillo II n8, Madrid 28108, Spain

HIGHLIGHTS

- Gage factor values at temperature up to 60 °C quadrupled the value of 20 °C tests.
- Temperature time history modified the strain sensing response after 60 °C heating.
- Maximum gage factor was obtained drying the material up to a 71% saturation degree.
- Low and constant gage factors were measured between 20 and 50% saturation degrees.
- Totally dried paste showed higher GF related to temperature-damage during drying.

GRAPHICAL ABSTRACT

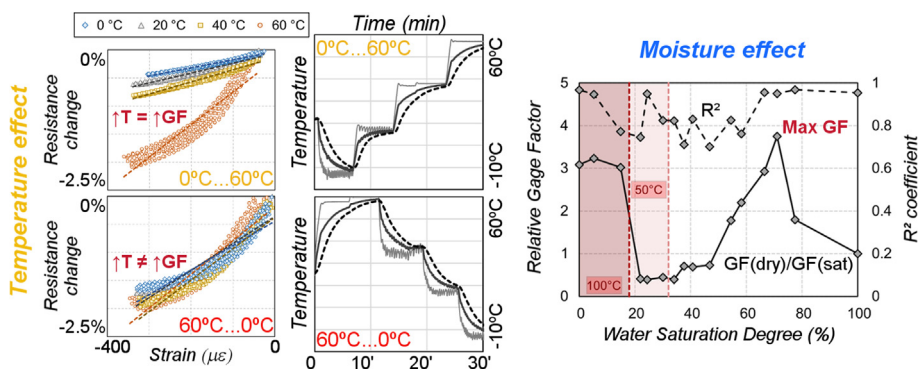

ARTICLE INFO

Article history:
Received 18 January 2021
Received in revised form 16 February 2021
Accepted 18 February 2021
Available online 8 March 2021

Keywords:
Cement composites
Multi-walled carbon nanotubes
Graphite
Hybrid fillers
Strain-sensing
Electrical resistivity
Temperature
Moisture

ABSTRACT

Cement composites with hybrid conductive fillers carbon nanotubes (CNT) and graphite products (GP), have been tested as strain sensors under varying temperatures (0 °C–60 °C), and moisture conditions (0%–100% saturation degree (SD)). Cement pastes with 1% CNT and 5% GP (purified expanded graphite) presented resistivity values between 50 and 75 Ohm·cm, and their strain sensing response was observed to be independent of the loading conditions. However, the gage factor increased up to four times for higher temperatures, and was influenced by the temperature time history. Gage factors were also increased when drying the material up to a SD of 71% or with entirely dried samples.

1. Introduction

Structural health monitoring systems could be design to control the performance of a structure to warrant safety and a proper service life, or also to optimize retrofitting interventions [1]. Despite the multiple typologies of strain sensors (piezoelectric ceramic sensors, optic fiber sensors, or strain gages), their durability is limited [2–4]. Cement based sensors appeared as an interesting alternative, and can be easily obtained by doping the cement matrix with a conductive admixture, e.g. carbon fibers (CF), nanofibers (CNF) or nanotubes (CNT) [5–7]. The addition of

* Corresponding author.
E-mail address: pedro.garces@ua.es (P. Garcés).

https://doi.org/10.1016/j.conbuildmat.2021.122786
0950-0618/

a conductive material improves the electrical conductivity of the composite, becoming a multifunctional material that can be applied to many other functionalities, such as deicing or as anode in electrochemical techniques [8–11]. The possibility of correlating the changes in the materials resistivity with their strain (and consequently stress and loads) makes them undoubtedly interesting for structural health monitoring purposes. This property is commonly known as strain-sensing and has been vastly studied over the last years [12–17].

The response of a sensor (strain gages or optic fiber) is usually affected by temperature, which should be controlled for an accurate strain measure. In addition, the need to achieve an adequate workability of the fresh mix usually implies the overdose of water, compared to what is strictly necessary to fully develop the hydration reactions. Hence, capillary porosity is developed, which is, responsible for the transport of aggressive substances phenomena, and ultimately the electrical conductivity of plain concrete. There are only a few studies that address temperature and moisture effects combined, in cement based sensors [18,19]. The electrical conductivity of a cement composite is a combination of electrolytic and electronic conductions, corresponding to the pore solution and conductive admixture respectively, and also tunnel effect between close conductive fibers or particles. The electrolytic conductivity largely depends on the degree of saturation and the temperature. Nevertheless, Dong et al. [20] concluded that the strain sensing capacity of a cement composite with carbon black addition was not significantly affected by temperature changes between 20 °C and 100 °C. On the other hand, Demircilioglu et al [21] detected that differences in thermal expansion coefficients between brass fibers and cement matrix may produce internal microcracks that affect the strain sensing response. Allam et al. [22] used partially dried cement composites in order to improve the strain sensing response of the material. Despite there is not a consensus on the strain sensing response affected by humidity changes, it is clear that very despair results will be obtained depending on the water saturation degree [23].

Regarding the design of the strain-sensing material itself, hybrid filler reinforcement is used to combine properties of one or more fillers in the composite. The use of filler materials with different sizes (e.g. fibers with high aspect ratio and particles), can reduce the amount of material necessary to achieve percolation, and potentially improve their strain-sensing response [24,25]. Besides, additions like CNT or carbon fibers are usually costly, while conductive particles can be byproducts from industrial processes, therefore a double benefit can be obtained minimizing costs and recycling wastes [26]. There are different studies that report an improvement in the piezoresistive response of hybrids with fibers of different size (CF and CNT) from the point of view of results and repeatability [27,28]. On the other hand, Konsta-Gdoutos and Aza [29] studied the sensing function in cementitious composites with the hybrid addition of both CNT and CNF for an amplified strain sensitivity of the material. Loamrat et al. [30] reported the effect of carbon fiber and graphite powder on resistivity of cement-based sensor under compression. Finally, Alonso and Puentes [31] demonstrated the self-protection and self-sensing functionalities of self-compacted concrete containing carbon nanotubes (CNT) and carbon microfibers (CMF) as hybrid system.

This work is part of a research project aimed at the development of nano-engineered cement composites with functional application in transport infrastructures. In order to develop strain sensors, conductive cement pastes with the hybrid addition of CNT and graphite (GP) were selected based on their respective good results in other applications [10,32]. Once the electrical conductivity had been optimized by testing different types of graphite and different dosages of GP and CNT, the strain sensing response of the material was characterized under different conditions. The strain sensing response at different temperature (between 0 °C and 60 °C) was tested. And the influence of internal humidity content was studied at different water saturations degrees (SD), first with saturated samples (100%SD) and progressively drying until specimens were totally dried (0%SD). Both studies were designed to give a wide range of external conditions, in order to simulate real service scenarios for the developed sensors.

2. Materials and methods

2.1. Materials and specimen's preparation

The experimental campaign of this research was divided into four different studies. First, the influence of the conductive admixtures on the resistivity of the composites was assessed in order to define an adequate proportion of conductive admixtures of the hybrid composite. Once the composite's dosage was defined, its strain sensing capacity was studied under different loading conditions. The third and fourth stages were focused on the assessment of the effect of temperature and water content in the strain sensing response of the hybrid composites.

For this purpose, different cement composites were prepared with a combination of two conductive nano-additions, carbon nanotubes (CNT) and graphite particles. All cement pastes were prepared with Portland cement type UNE-EN 197-1 CEM I 52.5R (supplied by Cemex España S.A.), distilled water and superplasticizer Sika Viscocrete 20-HE. The conductive admixtures were CNT type Graphistrength C100 supplied by Arkema (see main characteristics in Table 1), and graphite products (GP) supplied by Superior graphite (type ABG1010 and 2939APH (Table 2 includes a summary of their main properties). Initially, in order to determine the effect of each conductive admixture in the electrical resistivity, cement pastes were prepared with CNT content between 0% and 2% (with respect to cement mass), or graphite particles between 0% and 10% (with respect to cement mass). All these dosages maintained a water/cement ratio of 0.5, and the superplasticizer dosage was slightly modified to adjust the fresh mix workability. Afterwards, different hybrid combinations of CNT and a single type of graphite were tested. Finally, in the strain sensing study, the optimal dosage based on prior results was selected, which included 1% of CNT and 5% of ABG1010, and a w/c ratio of 0.4.

The correct dispersion of CNT in the cement matrix has a very significant importance in the electrical conductivity and sensing response of the composite [33,34]. To guarantee a proper dispersion of the nano-additions in the cement matrix a previously tested method was applied [35,36]. Before including CNT in the mix a two-step procedure was followed. First, CNT were poured with part of the mixing water in a shear mixer for ten minutes, then they were treated with an ultrasonic device (type Hielscher UP200S) for another ten minutes. The graphite products (ABG1010 and 2939APH) were only treated with ultrasounds. Once the conductive additions had been dispersed in water, the mixing procedure in the European Standard UNE-EN 196–3:2017 was used

Table 1
Main properties of CNT (provided by Arkema).

Description	CCVD Multi-wall Carbon Nanotubes	
Appearance	Black powder	
Powder characteristics	Apparent density	50–150 kg/m^3
	Mean agglomerate size	200–500 μm
	Weight loss at 105 °C	<1%
CNT characteristics	C content	>90 wt%
	Free amorphous carbon	Not detectable (SEM/TEM)
	Mean number of walls	5–15
	Outer mean diameter	10–15 nm
	Length	0.1–10 μm

Table 2
Graphite products: Purified Expanded Graphite ABG1010 and Purified Natural Flake Graphite 2939APH (provided by Superior Graphite).

Graphite Product	ABG1010	2939APH
Appearance	Black powder	Black powder
True density (g/cm^3)	2.25	2.25
Surface Area BET (m^2/g)	22	9
LOI	99.95%	99.95%
C content	>90 wt%	>90 wt%
Particle Size Distribution d10 (μm)	3.3	3.9
Particle Size Distribution d50 (μm)	9.8	9.0
Particle Size Distribution d90 (μm)	40.2	16.9

to prepare the cement pastes. After mixing the materials for five minutes, the paste was poured into prismatic molds to fabricate 4x4x16 cm^3 specimens, which were kept for 24 h in controlled environment (20 °C and relative humidity > 95%). Afterwards all specimens were demolded and kept in the same temperature and humidity conditions to fulfill a 28 days curing period.

2.2. Experimental tests in laboratory conditions

The electrical resistivity of the specimens was measured as shown in Fig. 1. Four electrical contacts were wrapped around the cross sections. Each electrode comprised a silver paint coating and a copper wire to make the connection with the electronic devices. A DC current source was connected to the outer electrodes, while the voltage between the inner electrodes was registered using a digital multimeter. Hence, electrical resistance can be calculated applying the Ohm's law, and resistivity can be obtained considering the specimen's geometry (length and cross section).

In the strain sensing tests, the load was applied in the longitudinal direction of the sample. The electrical resistance was obtained as shown in Fig. 1, and the mechanical response was controlled with a strain gage attached to the middle section to measure longitudinal strains. The sensing capacity is usually evaluated by means of the gage factor (GF), which is defined as the electrical resistivity change to strain ratio, as defined in eq. (1).

$$GF = (\Delta\rho/\rho_0)/\varepsilon \approx (\Delta R/R_0)/\varepsilon \tag{1}$$

where ΔR and $\Delta\rho$ are the change on electrical resistance and resistivity respectively; R_0 and ρ_0 are their corresponding initial values; and ε is the longitudinal strain. It is commonly accepted that the change in resistivity and resistance may be equivalent, as the effect of the dimensional changes in the sample may be negligible. Nonetheless in a preliminary approach, the influence of the strain field was assessed considering that uniaxial stress state was applied to the sample:

$$T = \begin{bmatrix} \sigma_x & 0 & 0 \\ 0 & 0 & 0 \\ 0 & 0 & 0 \end{bmatrix} = \begin{bmatrix} F/A & 0 & 0 \\ 0 & 0 & 0 \\ 0 & 0 & 0 \end{bmatrix} \tag{2}$$

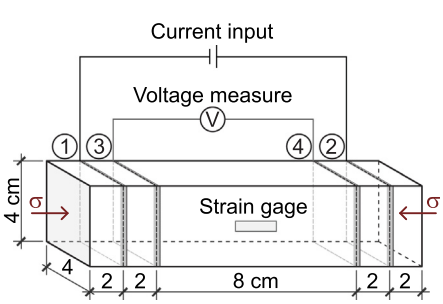

Fig. 1. Electrical contacts for resistivity measure of 4x4x16 cm^3 specimens.

where σ_x is the longitudinal stress (axial force F/cross section area A). Therefore, applying the Hooke's law, the strains in the three directions $\{\varepsilon_x, \varepsilon_y, \varepsilon_z\}$ can be easily obtained knowing the elastic modulus E and the Poisson's ratio ν of the material:

$$D = \begin{bmatrix} \varepsilon_x & 0 & 0 \\ 0 & \varepsilon_y & 0 \\ 0 & 0 & \varepsilon_z \end{bmatrix} = \begin{bmatrix} \sigma_x/E & 0 & 0 \\ 0 & -\nu\sigma_x/E & 0 \\ 0 & 0 & -\nu\sigma_x/E \end{bmatrix} \tag{3}$$

Then, deformations of the longitudinal and transverse dimensions can be obtained according to Eq. (4) to account for the changes of the geometry of the samples, and their influence on the observed resistivity changes.

$$\begin{aligned} \Delta l_x &= \int_0^{Length} \varepsilon_x \mathrm{d}x = \tfrac{\sigma_x}{E} l_x \\ \Delta l_y &= \Delta l_z = \int_0^{width} \varepsilon_y \mathrm{d}x = -\nu \tfrac{\sigma_x}{E} l_y \end{aligned} \tag{4}$$

2.3. Evaluation of the environmental conditions on the strain sensing response

After the characterization of the strain sensing capacity of the hybrid cement composites, the effect of temperature and water content of the material was evaluated. Fig. 2 shows the experimental setup for the tests with controlled temperature. Samples were tested in a mechanical press with a thermally insulated chamber, model MUF 401, supplied by Servosis. The air temperature inside the chamber can be controlled in the range between −10 °C and 150 °C. The electrical resistivity was monitored as previously explained in the tests with laboratory conditions. Besides the strains related to the applied stress, samples suffered additional thermal strains due to temperature changes. Hence, in order to control this effect a second specimen was put into the chamber. This sample was not loaded, and its strain gage registered only the thermal strains, which can be eliminated from the measured of the loaded specimen. In addition, ambient temperature and surface temperature of both specimens was measured with Pt-100 type temperature sensors. Also in the control sample a small drill was made to put a thermocouple in its center to control possible thermal gradients. In order to limit the effect of water loss related to sample's heating, the temperatures were fixed between 0 °C and 60 °C (with 20 °C increments).

Finally, the effect of water saturation was studied. For this purpose, samples were initially saturated and progressively dried in different conditions (40 °C, 50 °C and 100 °C). During this process, the following properties were controlled: water loss, electrical resistivity, elastic modulus and strain sensing response.

3. Results and discussion

3.1. Effect of conductive admixtures in the conductivity of cement matrices

Before preparing any hybrid cement composite (with CNT and GP) the effect of all three conductive materials as the sole doping admixture was addressed. In order to optimize the dosage of a conductive admixture, the percolation phenomena was studied.

The first goal of this study was to carry out preliminary compatibility tests between the carbon-based materials considered in this research, CNT and GP, and the addressed cement matrices. The electrical percolation threshold (EPT) can be defined as the necessary amount of conductive material (CNT or GP in this case) to create a continuous path for the electrical current. When percolation phenomena begins, the electrical resistivity of the composite drops several orders of magnitude for increasing CNT or GP volumes. When percolation ends, it would be useless to increase the

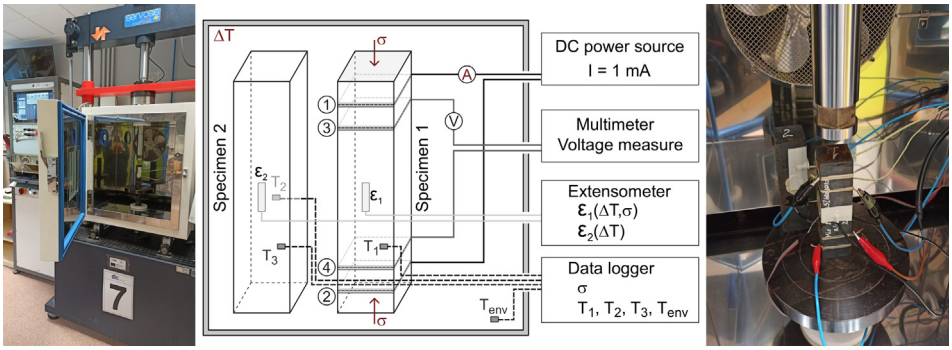

Fig. 2. Experimental setup for strain sensing tests with temperature control. Press with thermally insulated chamber for the tests of one sample, while monitoring the thermal strains of a second specimen.

CNT or GP amount because conductivity is not significantly changed anymore [37]. Fig. 3 shows the effect of CNT content in the material's resistivity for cement pastes tested just after the 28-days curing period. Percolation started at CNT dosages beyond 1% (with respect to cement mass). At that point, the addition of another conductive particle (usually waste or cheaper materials) can be used to benefit from the synergy between both materials as proven with different types of materials, even non-carbon additions [38]. In this case, the objective was to include GP in order to reduce the CNT amount necessary to obtain high conductivity.

On the other hand, cement pastes with purified expanded graphite (ABG1010) or purified natural flake Graphite (2939APH) were tested to observe their influence on the overall resistivity. In this case, besides the resistivity measurements after the water-saturated curing of 28 days, samples were kept in laboratory conditions and samples were naturally dried during another month. The difference in the aspect ratio of GP with respect to CNT makes more difficult to establish electronic conductive paths, and the resistivity of the material is more influenced by the electrolytic conduction of the pore solution [39]. Fig. 4 summarizes the effect of both types of GP in the conductivity at each humidity condition. First, if the saturated specimens after the curing are compared, an increase of GP% could not be directly related to an improvement of the conductivity of the composite. The addition of GP highly modifies the consistency and workability of the resulting mixes. Despite the superplasticizer amount was adjusted between batches, workability differences were observed. Therefore, the internal pore distribution and overall porosity could have been affected, and both factors influence the aforementioned electrolytic conduction. Compared with the control sample, only the

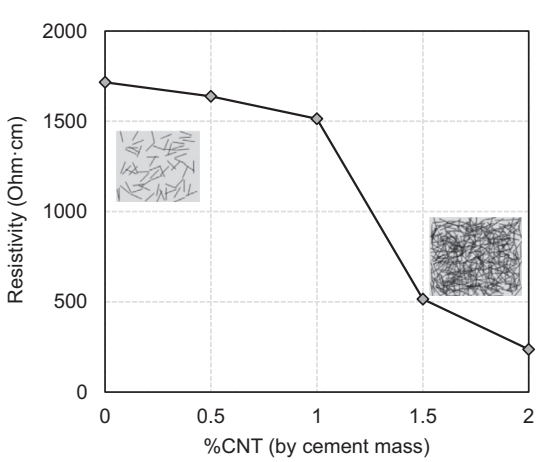

Fig. 3. Percolation threshold curves corresponding to cement paste specimens with different percentages of CNT. Curing time: 28 days.

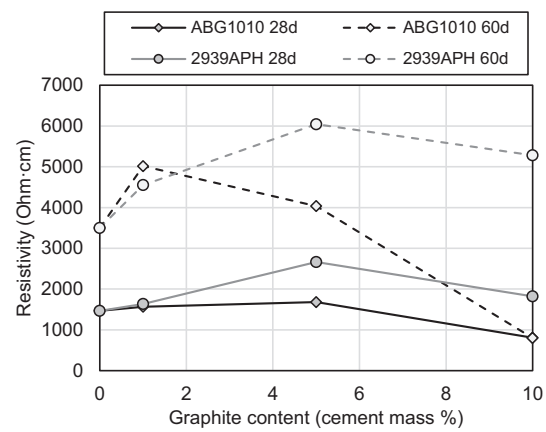

Fig. 4. Resistivity values of cement paste obtained with the addition of different graphite products after 28 days of water saturated curing and 21 days in laboratory conditions (22 °C and 60% RH).

dosage with 10% of ABG1010 could reduce the electrical resistivity in saturated conditions. An explanation should be found in its particle size and surface area BET (m^2/g), as shown before in Table 2, in which ABG1010 particles are bigger and has 22 m^2/g against only 9 m^2/g for the 2939APH. Consequently, the probability of contact between graphite particles was higher and therefore its value of resistivity decreases. A more important effect of ABG1010 can be found in the partially dried measurements. Logically, samples with a conductivity ruled by their electrolytic component may be more sensitive to humidity changes. In Fig. 4 a systematic resistivity increase was observed for all samples (especially if 2939APH was used). The only exception was the dosage with 10% of ABG1010, which maintained the same conductivity (808 vs. 802 Ohm·cm). Hence, ABG1010 was proven efficient to create more stable electric conduction, and would be used to prepare hybrid composites.

The next step of the research was to explore the possibilities of hybrid additions of CNT and GP, in order to improve the electrical properties of the composites, and their functional applications (strain sensing in this case). Binary combinations of 1%CNT and 5%GP were prepared and tested in different situations, just like the aforementioned samples with only GP addition. The objective of applying these materials as strain sensors requires that the electrical response of the material were as stable as possible in time. Hence, in this case, the electrical conductivity was measured after one and two months of natural drying in laboratory conditions. Fig. 5(a) includes the results of a control sample without any conductive admixture, and two batches with 1%CNT and 5%GP (both graphite types were tested). The resistivity of the control sample was the highest value at all conditions, and was highly increased during the drying process. The dosage with 2939APH

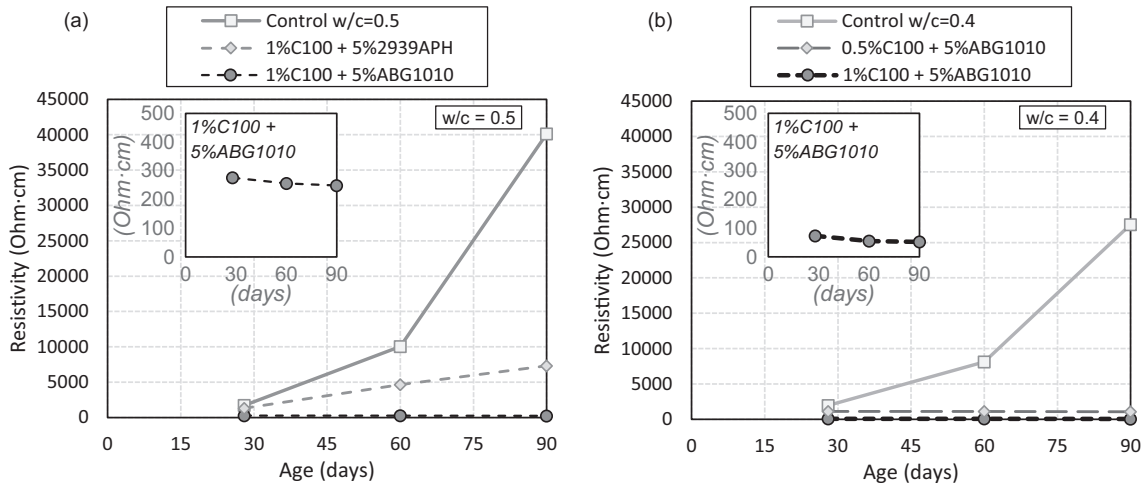

Fig. 5. Time evolution of the resistivity of cement pastes obtained with hybrid combinations of CNT and GP. All samples were cured in water saturated ambient for 28 days, and dried naturally in laboratory conditions (22 °C and 60% RH) until 60 and 90 days.

was capable of improving slightly the material's conductivity, but was still experiencing a linear increase over time. The most suitable addition was the combined use of CNT and ABG1010, which confirmed the conclusions drawn in Fig. 4. The electrical resistivity of a composite with 1%CNT and 5%ABG1010 showed a resistivity value below 300 Ohm·cm, even it decreased slightly when drying and was stabilized at 250 Ohm·cm approx. This conductivity stability of cement composites with time has been previously observed in dosages with strong electronic conduction, e.g. using carbon fibers as conductive enhancer [40]. Based on these results, ABG1010 was confirmed as the GP type to prepare the hybrid composites combined with CNT.

One final change was tested in the design of the hybrid composite, which comprised the effect of reducing the w/c ratio from 0.5 to 0.4, and checking if CNT dosage could be reduced even more without significant resistivity increase. Fig. 5(b) includes the time evolution of the resistivity of three batches (control without additions, 0.5%CNT + 5%GP and 1%CNT + 5%GP). The dosage with only 0.5% CNT improved only a little the conductivity of the control dosage in saturated conditions (from 1966 Ohm·cm to 1122 Ohm·cm), but was stable to during drying and did not suffer the resistivity increase shown by the control batch. The stable resistivity value around 1100 Ohm·cm could be interesting for some functional applications. On the other hand, the dosage with 1%CNT and 5%

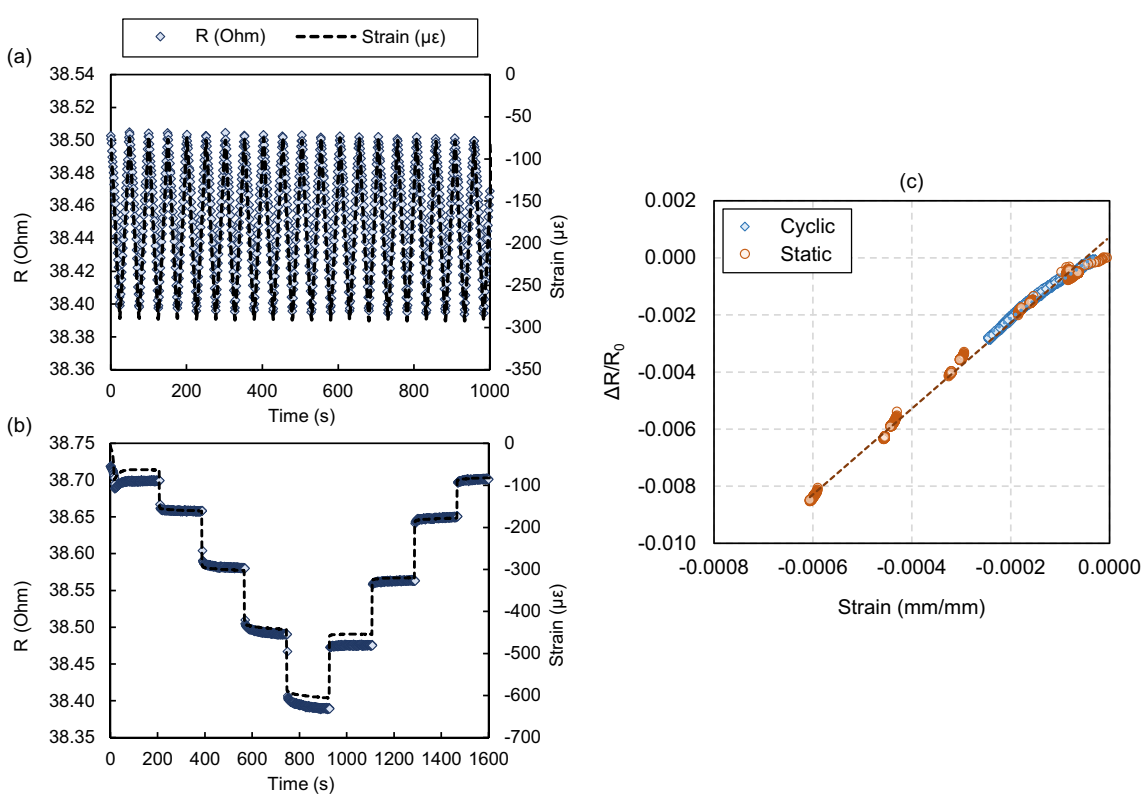

Fig. 6. Self-sensing tests for cement pastes doped with hybrid fillers, 1%CNT and 5%GP (type ABG1010) after 28 days of water saturated curing: resistivity and strain time histories for (a) compressive cyclic loading and (b) static constant loads; (c) resistance fractional change ($\Delta R/R_0$) versus strain of both tests.

GP was the most conductive of all tested in this research, 53 Ohm·cm after two-months drying. The reduction of w/c ration from 0.5 to 0.4 led to composites with higher conductivity, as the electrolytic component of conductivity is limited with lower water content and the electronic conduction given by CNT and GP prevails.

3.2. Self-sensing behavior of hybrid CNT and GP cement pastes

After the preliminary resistivity study, only one dosage was selected due its combined low resistivity value and its time stability when drying in laboratory conditions. Therefore, all the following results regarding the strain sensing characterization and the effect of temperature and moisture changes, would be referred to a cement paste with 1% of CNT and 5% of ABG1010 (with respect to cement mass) and a water to cement ratio of 0.4.

Fig. 6 includes the first strain-sensing test results when loads were applied in a different pattern (cyclic and static). In Fig. 6(a) cyclic loads were applied at a constant 200 N/s loading rate, while the test in Fig. 6(b) comprised different load levels in which each stress was maintained for 180 s. The maximum stress in the cyclic test was 4.06 MPa (equivalent to an axial force of 6.5 kN), and the steps in the second test were fixed at 0.94 MPa (1.5 kN), 2.19 MPa (3.5 kN), 4.06 MPa (6.5 kN), 5.94 MPa (9.5 kN) and 8.13 MPa (13.0 kN). During both tests, the electrical current was fixed at 1 mA while the changes in the resistance were monitored. In the time history functions in Fig. 6(a) and Fig. 6(b) the evolution of the electrical resistance follows the pattern of the induced longitudinal strains, and both of them were totally reversible when unloading. In Fig. 6(c) both responses have been compared, but this time fractional changes of resistance versus longitudinal strains were represented, in which the gage factor (GF) can be directly obtained with a linear regression analysis (represented as a dark dashed line). Both tests presented a very similar behavior, with an average GF of 12.8 (cyclic load) and 15.0 (static load). This slight difference can be explain by the difference in the maximum stress, which in the static test was twice the value of the cyclic test. Similar increases in GF for progressively higher load levels had been previously reported [13,14]. Some points in Fig. 6(c) corresponding to the static test did not adjust to the overall behavior. These data correspond to measurements taken during the loading between different steps, which was made at a much higher loading rate affecting the electrical–mechanical correlation at those particular points.

Before further analysis, Eqs. (2) to (4) were applied to quantify the fraction of the strain sensing response that could be justified by dimensional changes (i.e. longitudinal contraction and transverse elongation for a longitudinal compressive stress). Fig. 7(a) compares the experimental resistance change measured in a cyclic loading test and the equivalent with the changes obtained from the aforementioned equations. In this case the Poisson's ratio of the material was undetermined, so three different values have been represented, first the limit values of 0 and 0.5 and a typical value for cement materials like 0.2. Nonetheless, the ratios between the theoretical and experimental values for each Poisson's ratio have been represented in Fig. 7(b), and the average electrical response that could have been justified due to dimensional changes was approximately 10% of the total response observed in the strain sensing tests.

A preliminary calibration process was made to control if the material's response was stable under different combinations of maximum stress (4.06 and 8.13 MPa) and loading rate (100, 200 and 400 N/s). Fig. 8 includes all the resistance change vs. longitudinal strain for the combinations of both variables. In general, all tests resulted in a similar behavior with an average GF of 14.1 ± 1.4, which was obtained by linear regression of the data of each test separately. In addition, there was the aforementioned effect of the maximum load level, with GF of 13.0 for a 6.5 kN load and 15.2 for 13 kN. Similar trends in GF with increasing loads have been reported in [13,14].

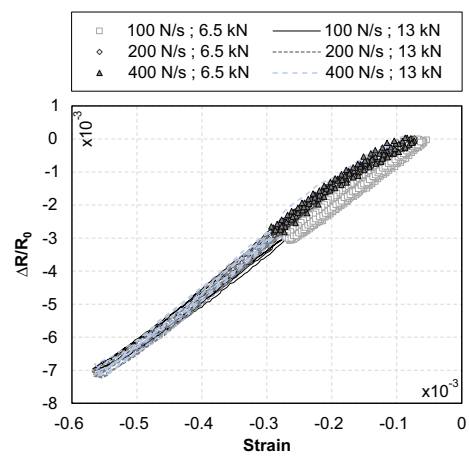

Fig. 8. Self-sensing tests for cement pastes doped with hybrid fillers, 1%CNT and 5% GP (type ABG1010) after 28 days of water saturated curing: resistance fractional change ($\Delta R/R_0$) vs. strain for different combinations of maximum stress and loading rate.

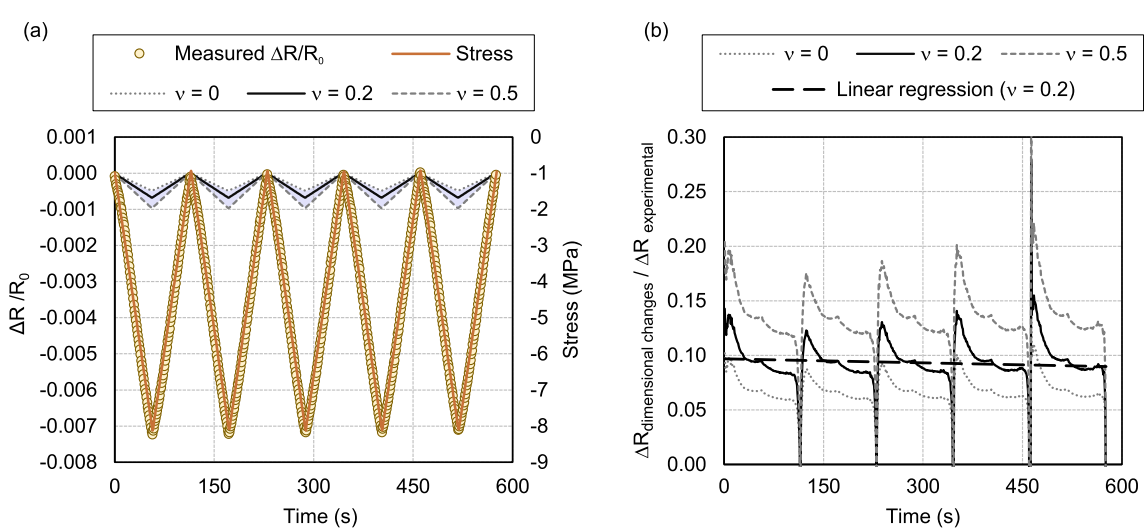

Fig. 7. Effect of dimensional changes on the strain sensing response: (a) time evolution of the experimental measure and the theoretical resistance changes related to geometrical deformations for different Poisson's ratios; (b) ratio between the theoretical and experimental resistance changes.

3.3. Effect of temperature in the strain-sensing response

The next step in the strain sensing characterization was to establish the influence of the environmental conditions in the response of the hybrid composites with 1% CNT and 5% ABG1010. First, the influence of the temperature was studied between 0 °C and 60 °C. Table 3 summarizes the relevant parameters in tests made on different days, in which samples were kept in ambient temperature, and then tested as shown in Fig. 2. Only one heating or cooling ramp was made each day, and after the strain sensing tests, samples returned naturally to ambient temperature. There was a very slight resistivity increase with temperature, from 43.7 Ohm·cm at 0 °C to 45.7 Ohm·cm at 60 °C. In other work, also no significant changes in the conductivity were reported in the interval between 50 and 115 °C [21]. The mechanical response was similar in all tests, with elastic modulus between 23 and 26 GPa (discarding any structural damage during the loading or heating processes). However, there were severe changes in the strain sensing response and the GF at 60 °C was four times the GF at 0 °C. A clear increasing trend was observed in the GF upon heating, especially in the last temperature level. No specific measure was taken to avoid moisture interchange between samples and the environment. In prior research [41], 60 °C was determined to be a turning point for this moisture changes, and during self-heating tests it was observed that pore-water in cement materials could undergo a change of state and begin to evaporate. This modification of the pore solution may have affected the balance between electrolytic and electronic conductions, enhancing the strain-sensing performance of samples after small drying [22,42,43]. In addition, according to Shifeng et al. [44], temperature may increase the tunneling effect in the range below 100 °C, because electrons transform heat energy to kinetic energy. Beyond the limit of 100–130 °C internal pore pressure due to increasing water vapor resulted in higher resistivity values. In our case, samples were heated to a maximum temperature of 60 °C, with the consequent surface drying. Therefore, electron's mobility was increased because of better electronic conduction and tunneling effect, which may have resulted in the enhanced strain-sensing response at said temperatures.

Fig. 9 summarizes the experimental results of strain sensing tests, made in samples under a progressive heating or cooling pro-

Table 3
Effect of temperature on different electromechanical parameters during strain sensing tests: electrical resistivity, elastic modulus, gage factor and R^2 Pearson coefficient of the linear regression.

Temperature	Electrical resistivity (Ohm·cm)	Elastic modulus (GPa)	Gage Factor	R^2
0 °C	43.70	26.2	14.3	0.968
20 °C	43.80	26.0	17.4	0.971
40 °C	44.18	23.6	22.3	0.975
60 °C	45.70	23.1	58.8	0.888

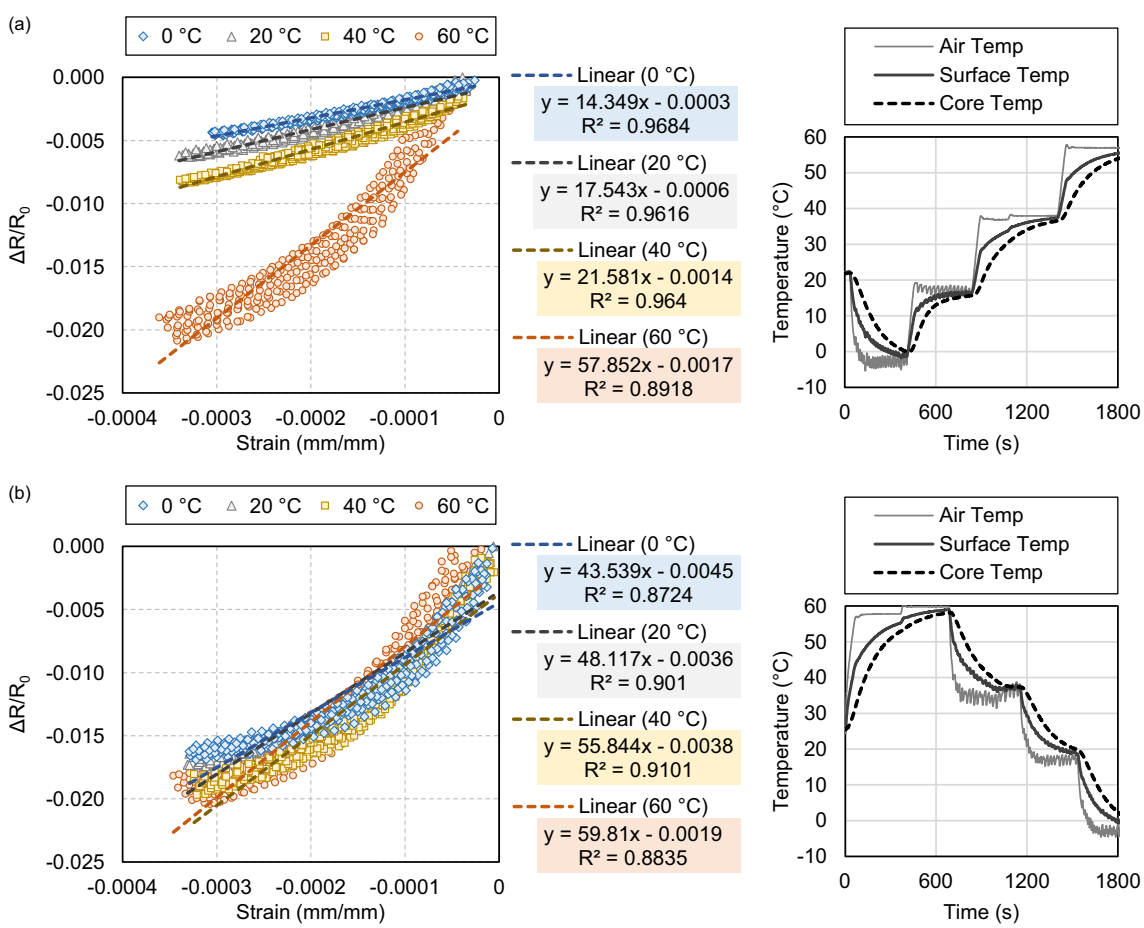

Fig. 9. Strain sensing results (resistance change vs. strain) and temperature time history for tests made on cement pastes with 1%CNT and 5%GP at temperatures between 0 °C and 60 °C with different temperature protocol: (a) heating or (b) cooling.

cess. In these experiments, all temperature levels were tested on the same day as shown in the temperature curves. Once the temperature on the surface of the sample was stabilized to the target value the strain sensing test was carried out, and heating–cooling continued afterwards. The response of the samples in the heating set, Fig. 9(a), was almost identical to the individual tests reported in Table 3. In this sequence, samples were cooled to 0 °C and heated after in 20 °C steps up to a maximum temperature of 60 °C. The gage factor and linearity (R^2 coefficient) of the response were maintained. Only the sample at 60 °C seemed to present a small non-linear effect, but the linear regression function still presented a R^2 value of 0.89. On the other hand, the response was quite different when samples were first heated to 60 °C and then progressively cooled to 0 °C, as shown in Fig. 9(b). The GF for a 60 °C temperature was similar to the corresponding values in Fig. 9(a) and Table 3. However, the response at lower temperatures have been drastically modified (GF values in the range of 14–22 were increased to 43–56, and linearity was also slightly reduced). The combined effect of moisture and temperature should be discussed at this point. First, tests were controlled based on the surface temperature of the specimens, but there was a gradient between the outer and inner temperatures. The measurementss of three thermocouples were represented in the temperature time history functions of Fig. 9. One corresponded to the air temperature inside the chamber, other to the surface temperature of the specimen, and the last one to the temperature of the central point of the sample. When the ambient had reached the target temperature for the strain sensing tests, it was maintained for 10 min approximately until the surface temperature was equal to the air temperature. At that point, there was actually a small gradient with the core of the sample, which was smaller when heating, and higher when cooling. Nonetheless, this temperature difference was always below 2 °C at the beginning of the strain sensing tests. Therefore, the change in the behavior of samples at 40 °C and below should not be only temperature related, as those temperature changes between Fig. 9(a) and (b) did not seem significant.

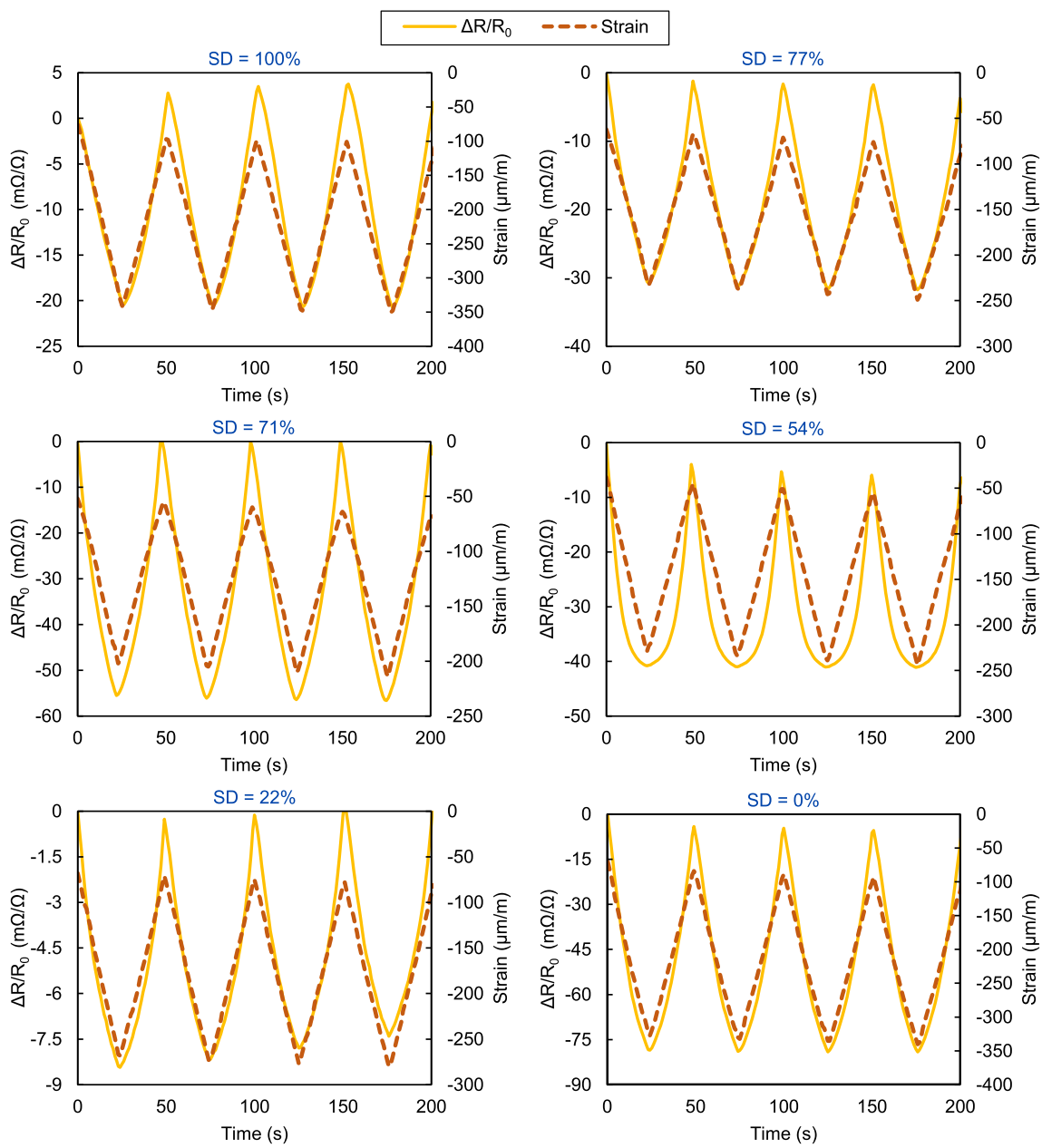

Fig. 10. Strain sensing tests (resistance change and strain vs. time) of cement pastes with 1%CNT and 5%GP (w/c = 0.4) at different saturation degrees between 100% and 0%.

The difference between both sets of tests may have been in moisture changes in the skin of the samples, which as stated above may occur at temperatures ≥ 60 °C. The aforementioned effects on the electronic/electrolytic conductions and tunneling effects may be related to the drying of the cement matrix rather than the temperature of the composite. Nonetheless, the overall mass changes during the tests were small, and so were the total modification of the saturation degree of the material. In the next stage of this work, the isolated effect of water content changes on the strain sensing response was studied, in order to uncouple it from the influence of the temperature in the phenomenon. However, samples in the temperature study were in especially sensitive humidity conditions, in which significant GF variations may be produced with small moisture modifications, as it will be discussed further on.

3.4. Effect of the water saturation degree in the strain-sensing response

In order to study the effect of the moisture content on the response of the composites, after being saturated, samples were progressively dried in controlled conditions. First, they were put in an electric oven at 40 °C, after at 50 °C (together with vacuum drying), and finally they were completely dried at 100 °C. During this process, the mass loss was controlled to determine the water saturation degree (SD), and the electrical resistivity and strain-sensing response was measure at each point. Before making any electrical measure, samples were kept in a desiccator with silica gel to cool, and were tested at ambient temperature, to avoid any temperature related effects. Fig. 10 includes the resistance change and longitudinal strain time-functions for eight different saturations degrees during this process. All of them showed an electrical response that could be correlated to the mechanical induced strains, unlike other composites with carbon fibers in which water saturated specimens didn't show a proper behavior [45]. However, in some points, obvious non-linear effects were registered, like in the test at 54% SD.

A detailed analysis of the results of all strain sensing tests at different SD can be found in Fig. 11. First, the electrical resistance presented a linear decreasing trend as the composite was drying, as shown in Fig. 11(a). The low resistance value (<30 Ohm) was a remark of the prevalence of the electronic conduction, which is by nature less affected by humidity changes in the matrix. In other works, there was a clear increase in samples' resistivity upon drying, but they were less conductive composites [21,46]. In order to achieve the total removal of internal moisture, the temperature of the oven was progressively increased. Therefore, the elastic modulus could give an idea of the structural integrity of the material exposed to those temperature levels. Also in Fig. 11(a) the evolution of the elastic modulus showed that after the first 24 h at 100 °C (to decrease SD below 20%) the elastic modulus decreased from 15 GPa to 10 GPa. There were several cracks on the materials surface after this temperature exposure, which should be considered in the interpretation of the strain sensing tests. Fig. 11(b) presents the sensitivity (GF) and linearity (R^2 coefficient) of all strain sensing tests made at ambient temperature. In this case, the GF has been represented as the relative gage factor with respect to the value of the saturated composite. The existence of a maximum GF value corresponding to an optimal SD has been reported also in other works with different materials [43,45]. In this case, there was an initial increase, in which GF was almost four times the saturated specimen's value. The maximum GF was obtained for a 71% SD, for example in [45] the optimum SD was around 50%. After that point the GF begun to decrease, even to relative values below 1. But also the linearity (R^2 Pearson coefficient) of the linear regression between the resistance change and the strain was affected. For saturation degrees higher than 65% the R^2 values were always > 0.95,

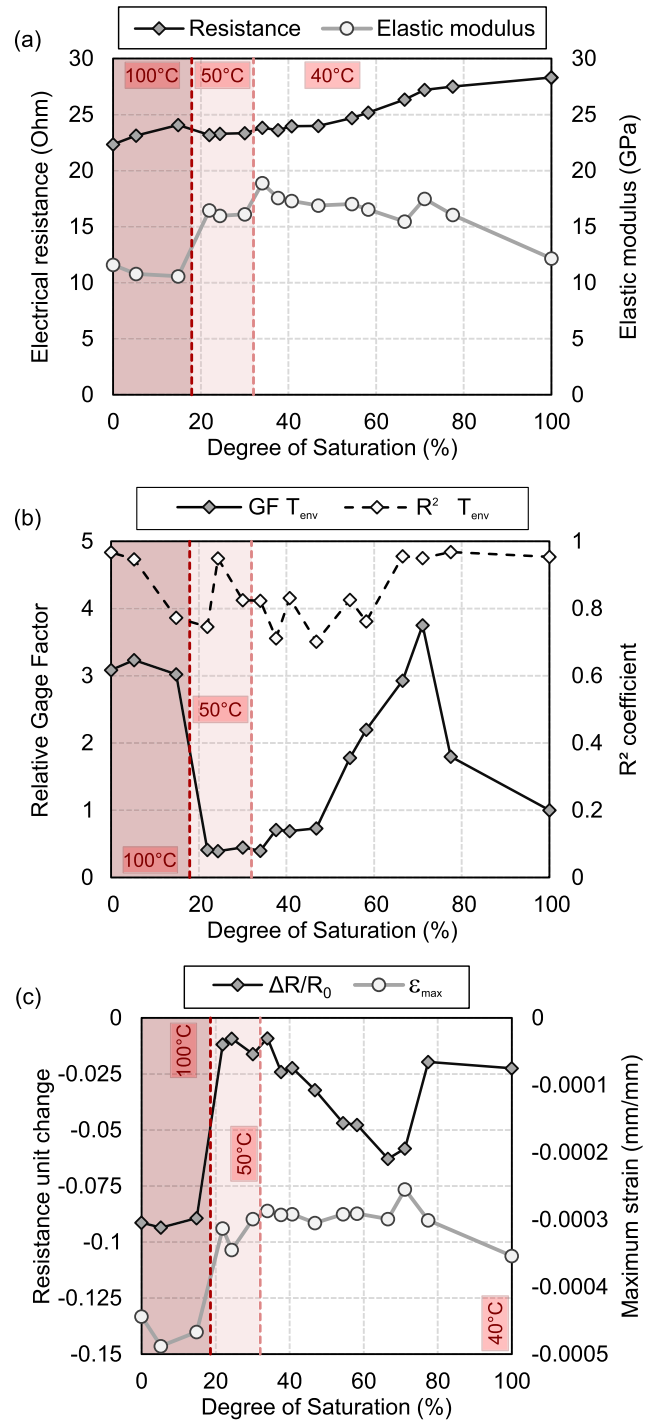

Fig. 11. Effect of drying (expressed as the water saturation degree) on different electromechanical and functional variables measured in strain sensing tests on cement paste with 1%CNT and 5%GP (type ABG1010). All tests were made at ambient temperature after drying inside an electric oven at 40 °C, 50 °C or 100 °C.

while drier samples presented values between 0.70 and 0.83, in most cases. There was another change of the GF trend after samples had been exposed to 100 °C, in which high GF were measured again. Fig. 11(c) shows the two variables responsible for the GF value, the resistance change of the material ($\Delta R/R_0$) and the longitudinal strain. The higher values measured during the whole strain sensing test for both magnitudes have been represented in Fig. 11 (c). Hence, an increase in $\Delta R/R_0$ would mean a higher GF, while higher strain values would refer to a reduced GF. In all measurements made during the 40 °C and 50 °C drying phases the changes

in GF could be directly related to the effect on the material's conductivity. As confirmed by the elastic modulus, the mechanical response of the material was not affected by temperature exposure and the level of strain was similar in all tests. Therefore, the changes in the gage factor respond to the aforementioned effects on the electronic or tunneling effect conductions. However, after a 100 °C exposure, the material was damaged (as shown by the decrease in elastic modulus) and the longitudinal strains were higher. Instead of a GF loss, it was increased because the change of resistance was highly affected. In that case, the electrolytic conduction had been totally removed, and the electrical response may have been magnified because the CNT had to act as bridges in all the internal cracks developed by temperature exposure. This higher sensitivity of dry specimens (0% humidity content) has been also recently reported in cement mortar with the addition of carbon nanofibers [46]. From the point of view of discrete sensors embedded or attached to a regular structure, the loss of mechanical performance (elastic modulus) may not be a problem. Nevertheless, if bulk sensing behavior of complete structural elements wanted to be developed, the first peak at higher internal humidity would be preferable. On the other hand, the magnified electrical response of a damaged material (cracked after 100 °C drying) may led to high-sensitive materials when this cracks are mechanical-stress related instead of thermal exposure, and could be a suitable damage sensing material.

4. Conclusions

Different hybrid cement composites made with a combined addition of carbon nanotubes (CNT) and graphite products (GP) were prepared in order to develop strain sensors and test their response under different environmental conditions (temperature and humidity). After the selection of the conductive additions (type and dosage), strain sensing tests were performed at controlled temperature conditions, and after samples had been progressively dried to modify their water saturation degree. Once all tests and the analyses presented above, the following conclusions may be drawn to summarize the most significant findings of the present study:

1. Percolation of CNT was observed for additions higher than 1.0%. When CNT and GP were combined, the hybrid composite could present resistivity values stable with time and humidity changes related to exposure to laboratory conditions for several months. When ABG1010 addition was the selected GP addition, the hybrid composite presented resistivity values between 50 and 75 Ohm·cm. Regarding the electrical resistance, the capacity of both CNT and GP (ABG1010) to act as electronic conductors in a cement matrix was observed.
2. In the stress levels tested in this research, cement paste specimens with 1%CNT and 5%ABG1010 showed good strain sensing properties, with a constant response regardless of the loading rate or maximum stress applied.
3. A temperature increase (between 0 °C and 60 °C) led to higher gage factor values in strain sensing tests. The sequence of testing may affect the strain sensing response of the material. If samples were tested after cooling from a prior higher temperature, the surface drying made during the first test still had influence in the second, resulting in bigger gage factor than expected.
4. When samples were subjected to a drying process, three different stages in the strain sensing response were distinguished. Initial drying of water saturated specimens led to an increased gage factor value until an optimal saturation degree of 70% approximately. Afterwards the electrical response of the material was reduced and non-linear effects appeared. In this stage, gage factor values were reduced even below the initial value of the saturated composite. Finally, after exposure to 100 °C, the material was damaged as shown by lower elastic modulus of elasticity. However, the gage factor was increased favored by an overall crack distribution because the thermal exposure.

CRediT authorship contribution statement

Beatriz del Moral: Formal analysis, Investigation, Writing - original draft, Visualization. **F. Javier Baeza:** Conceptualization, Methodology, Formal analysis, Writing - original draft, Visualization. **Rosa Navarro:** Investigation. **Oscar Galao:** Data curation, Writing - review & editing. **Emilio Zornoza:** Conceptualization, Writing - review & editing. **Jose Vera:** Supervision, Funding acquisition. **Catalina Farcas:** Investigation. **Pedro Garcés:** Conceptualization, Validation, Resources, Writing - review & editing, Supervision, Project administration, Funding acquisition.

Declaration of Competing Interest

The authors declare that they have no known competing financial interests or personal relationships that could have appeared to influence the work reported in this paper.

Acknowledgements

This project has received funding from the European Union's Horizon 2020 Research and Innovation Programme under grant agreement ID 760940, and from the Generalitat Valenciana grant AICO/2019/050.

References

[1] F.J. Baeza, S. Ivorra, D. Bru, F.B. Varona, Structural Health Monitoring Systems for Smart Heritage and Infrastructures in Spain, in: E. Ottaviano, A. Pelliccio, V. Gattulli (Eds.), Mechatronics Cult. Herit. Civ. Eng., Springer International Publishing, 2018: pp. 271–294. doi:10.1007/978-3-319-68646-2_12.
[2] H.-N. Li, D.-S. Li, G.-B. Song, Recent applications of fiber optic sensors to health monitoring in civil engineering, Eng. Struct. 26 (11) (2004) 1647–1657, https://doi.org/10.1007/978-3-319-68646-2_12.
[3] G. Song, Y.L. Mo, K. Otero, H. Gu, Health monitoring and rehabilitation of a concrete structure using intelligent materials, Smart Mater. Struct. 15 (2) (2006) 309–314, https://doi.org/10.1088/0964-1726/15/2/010.
[4] P.C. Chang, A. Flatau, S.C. Liu, Review Paper: Health Monitoring of Civil Infrastructure, Struct. Health Monitor. 2 (3) (2003) 257–267, https://doi.org/10.1177/1475921703036169.
[5] F. Azhari, N. Banthia, Carbon fiber-reinforced cementitious composites for tensile strain sensing, ACI Mater. J. 114 (2017), https://doi.org/10.14359/51689486.
[6] C. Camacho-Ballesta, E. Zornoza, P. Garcés, Performance of cement-based sensors with CNT for strain sensing, Adv. Cem. Res. 28 (4) (2016) 274–284.
[7] B. Han, S. Ding, X. Yu, Intrinsic self-sensing concrete and structures: a review, Measurement 59 (2015) 110–128, https://doi.org/10.1016/j.measurement.2014.09.048.
[8] D.D.L. Chung, Review functional properties of cement-matrix composites, J. Mater. Sci. 36 (2001) 1315–1324, https://doi.org/10.1023/A:1017522616006.
[9] B. del Moral, O. Galao, C. Anton, M.A. Climent, P. Garcés, Usability of cement paste containing carbon nanofibres as an anode in electrochemical chloride extraction from concrete, Mater. Constr. 63 (2013) 39–48, https://doi.org/10.3989/mc.2012.03111.
[10] J. Carmona, M.-Á. Climent, C. Antón, G. de Vera, P. Garcés, Shape Effect of Electrochemical Chloride Extraction in Structural Reinforced Concrete Elements Using a New Cement-Based Anodic System, Materials (Basel). 8 (2015) 2901–2917.
[11] O. Galao, L. Bañón, F. Baeza, J. Carmona, P. Garcés, Highly conductive carbon fiber reinforced concrete for icing prevention and curing, Materials 9 (4) (2016) 281, https://doi.org/10.3390/ma9040281.
[12] F. Ubertini, S. Laflamme, H. Ceylan, A. Luigi Materazzi, G. Cerni, H. Saleem, A. D'Alessandro, A. Corradini, Novel nanocomposite technologies for dynamic monitoring of structures: a comparison between cement-based embeddable and soft elastomeric surface sensors, Smart Mater. Struct. 23 (4) (2014) 045023, https://doi.org/10.1088/0964-1726/23/4/045023.
[13] F.J. Baeza, O. Galao, E. Zornoza, P. Garcés, Effect of aspect ratio on strain sensing capacity of carbon fiber reinforced cement composites, Mater. Des. 51 (2013) 1085–1094, https://doi.org/10.1016/j.matdes.2013.05.010.

[14] O. Galao, F.J. Baeza, E. Zornoza, P. Garcés, Strain and damage sensing properties on multifunctional cement composites with CNF admixture, Cem. Concr. Compos. 46 (2014) 90–98. doi:10.1016/j.cemconcomp.2013.11.009.
[15] F. Ubertini, S. Laflamme, A. D'Alessandro, Smart Cement Paste with Carbon Nanotubes, in: Innov. Dev. Adv. Multifunct. Nanocomposites Civ. Struct. Eng., 2016. doi:10.1016/B978-1-78242-326-3.00006-3.
[16] D.D.L. Chung, Self-monitoring structural materials, Mater. Sci. Eng.: R: Reports 22 (2) (1998) 57–78, https://doi.org/10.1016/S0927-796X(97)00021-1.
[17] F. Baeza, O. Galao, E. Zornoza, P. Garcés, Multifunctional cement composites strain and damage sensors applied on reinforced concrete (RC) structural elements, Materials 6 (3) (2013) 841–855, https://doi.org/10.3390/ma6030841.
[18] W. Dong, W. Li, Z. Tao, K. Wang, Piezoresistive properties of cement-based sensors: review and perspective, Constr. Build. Mater. 203 (2019) 146–163, https://doi.org/10.1016/j.conbuildmat.2019.01.081.
[19] Y. Wang, X. Zhao, Y.i. Zhao, Piezoresistivity of cement matrix composites incorporating multiwalled carbon nanotubes due to moisture variation, Adv. Civil Eng. 2020 (2020) 1–11, https://doi.org/10.1155/2020/5476092.
[20] W. Dong, W. Li, N.a. Lu, F. Qu, K. Vessalas, D. Sheng, Piezoresistive behaviours of cement-based sensor with carbon black subjected to various temperature and water content, Compos. B Eng. 178 (2019) 107488, https://doi.org/10.1016/j.compositesb:2019.107488.
[21] E. Demircilioğlu, E. Teomete, E. Schlangen, F.J. Baeza, Temperature and moisture effects on electrical resistance and strain sensitivity of smart concrete, Constr. Build. Mater. 224 (2019) 420–427, https://doi.org/10.1016/j.conbuildmat.2019.07.091.
[22] H. Allam, F. Duplan, J.-P. Clerc, S. Amziane, Y. Burtschell, About electrical resistivity variation during drying and improvement of the sensing behavior of carbon fiber-reinforced smart concrete, Constr. Build. Mater. 264 (2020) 120699, https://doi.org/10.1016/j.conbuildmat.2020.120699.
[23] F.J. Baeza, E. Zornoza, L.G. Andion, S. Ivorra, P. Garces, Variables affecting strain sensing function in cementitious composites with carbon fibers, Comput. Concr. 8 (2) (2011) 229–241.
[24] X. Fan, D. Fang, M. Sun, Z. Li, Piezoresistivity of carbon fiber graphite cement-based composites with CCCW, J. Wuhan Univ. Technol.-Mat. Sci. Edit. 26 (2) (2011) 339–343, https://doi.org/10.1007/s11595-011-0226-0.
[25] J. Luo, Z. Duan, T. Zhao, Q. Li, Self-sensing property of cementitious nanocomposites hybrid with nanophase carbon nanotube and carbon black, in: Adv. Mater. Res., 2011. doi:10.4028/www.scientific.net/AMR.143-144.644.
[26] F.J. Baeza, O. Galao, I.J. Vegas, M. Cano, P. Garcés, Influence of recycled slag aggregates on the conductivity and strain sensing capacity of carbon fiber reinforced cement mortars, Constr. Build. Mater. 184 (2018) 311–319, https://doi.org/10.1016/j.conbuildmat.2018.06.218.
[27] F. Azhari, N. Banthia, Cement-based sensors with carbon fibers and carbon nanotubes for piezoresistive sensing, Cem. Concr. Compos. 34 (7) (2012) 866–873, https://doi.org/10.1016/j.cemconcomp.2012.04.007.
[28] J.L. Luo, Z.D. Duan, T.J. Zhao, Q.Y. Li, Hybrid effect of carbon fiber on piezoresistivity of carbon nanotube cement-based composite, AMR 143-144 (2011) 639–643, https://doi.org/10.4028/www.scientific.net/AMR.143-144.
[29] M.S. Konsta-Gdoutos, C.A. Aza, Self sensing carbon nanotube (CNT) and nanofiber (CNF) cementitious composites for real time damage assessment in smart structures, Cem. Concr. Compos. 53 (2014) 162–169, https://doi.org/10.1016/j.cemconcomp.2014.07.003.
[30] K. Loamrat, M. Sappakittipakorn, P. Sukontasukkul, N. Banthia, Effect of carbon fiber and graphite powder on resistivity of cement-based sensor under compression, KMUTNB: IJAST 7 (1) (2014) 29–35, https://doi.org/10.14416/j.ijast.2014.01.005.
[31] A. Maria Cruz, P. Javier, Self-compacted concrete with self-protection and self-sensing functionality for energy infrastructures, Materials 13 (5) (2020) 1106, https://doi.org/10.3390/ma13051106.
[32] J. Carmona, P. Garcés, M.A. Climent, Efficiency of a conductive cement-based anodic system for the application of cathodic protection, cathodic prevention and electrochemical chloride extraction to control corrosion in reinforced concrete structures, Corros. Sci. 96 (2015) 102–111.
[33] M.S. Konsta-Gdoutos, Z.S. Metaxa, S.P. Shah, Highly dispersed carbon nanotube reinforced cement based materials, Cem. Concr. Res. 40 (7) (2010) 1052–1059, https://doi.org/10.1016/j.cemconres.2010.02.015.
[34] P.A. Danoglidis, M.S. Konsta-Gdoutos, S.P. Shah, Relationship between the carbon nanotube dispersion state, electrochemical impedance and capacitance and mechanical properties of percolative nanoreinforced OPC mortars, Carbon 145 (2019) 218–228, https://doi.org/10.1016/j.carbon.2018.12.088.
[35] B. Del Moral, I. Martín Gullón, R. Navarro, O. Galao, F.J. Baeza, E. Zornoza, B. Calderón, I. Rodríguez, N. Arnaiz, M.D. Romero Sánchez, P. Garcés, The effect of different oxygen surface functionalization of carbon nanotubes on the electrical resistivity and strain sensing function of cement pastes, Nanomaterials 10 (4) (2020) 807, https://doi.org/10.3390/nano10040807.
[36] M. del Carmen Camacho, O. Galao, F. Baeza, E. Zornoza, P. Garcés, Mechanical properties and durability of CNT cement composites, Materials 7 (3) (2014) 1640–1651, https://doi.org/10.3390/ma7031640.
[37] P.A. Danoglidis, M.S. Konsta-Gdoutos, E.E. Gdoutos, S.P. Shah, Strength, energy absorption capability and self-sensing properties of multifunctional carbon nanotube reinforced mortars, Constr. Build. Mater. 120 (2016) 265–274, https://doi.org/10.1016/j.conbuildmat.2016.05.049.
[38] S. Yehia, C.Y. Tuan, D. Ferdon, B. Chen, Conductive concrete overlay for bridge deck deicing: Mixture proportioning, optimization, and properties, ACI Struct. J. 97 (2000) 172–181.
[39] C. Andrade, P. Garcés, F.J. Baeza, O. Galao, E. Zornoza, Electronic and electrolytic conduction of cement pastes with additions of carbonaceous materials, in: C. Andrade, J. Gulikers, R. Polder (Eds.), Durab. Reinf. Concr. from Compos. to Prot., Springer, 2015: pp. 11–25. doi:10.1007/978-3-319-09921-7.
[40] W. Chuang, J. Geng-sheng, L.i. Bing-liang, P. Lei, F. Ying, G. Ni, L.i. Ke-zhi, Dispersion of carbon fibers and conductivity of carbon fiber-reinforced cement-based composites, Ceram. Int. 43 (17) (2017) 15122–15132, https://doi.org/10.1016/j.ceramint.2017.08.041.
[41] J. Gomis, O. Galao, V. Gomis, E. Zornoza, P. Garcés, Self-heating and deicing conductive cement. Experimental study and modeling, Constr. Build. Mater. 75 (2015) 442–449. doi:10.1016/j.conbuildmat.2014.11.042.
[42] J.L. Vilaplana, F.J. Baeza, O. Galao, E. Zornoza, P. Garces, Self-sensing properties of alkali activated blast furnace slag (BFS) composites reinforced with carbon fibers, Materials (Basel). 6 (2013) 4776–4786. doi:10.3390/ma6104776.
[43] S. Wen, D.D.L. Chung, Effect of moisture on piezoresistivity of carbon fiber-reinforced cement paste, ACI Mater. J. 105 (2008) 274–280.
[44] H. Shifeng, X.u. Dongyu, C. Jun, X.u. Ronghua, L.u. Lingchao, C. Xin, Smart properties of carbon fiber reinforced cement-based composites, J. Compos. Mater. 41 (1) (2007) 125–131, https://doi.org/10.1177/0021998306063378.
[45] F.J. Baeza, J.L. Vilaplana, Ó. Galao, P. Garcés, Sensitivity study of self-sensing strain capacity of alkali-activated blast furnace slag reinforced with carbon fibres, Hormigón y Acero. 69 (2018) 243–250, https://doi.org/10.1016/j.hya.2017.04.008.
[46] H. Wang, A. Zhang, L. Zhang, Q. Wang, X.-H. Yang, X. Gao, F. Shi, Electrical and piezoresistive properties of carbon nanofiber cement mortar under different temperatures and water contents, Constr. Build. Mater. 265 (2020) 120740, https://doi.org/10.1016/j.conbuildmat.2020.120740.